https://doi.org/10.1016/j.energy.2016.08.005

Performance improvement of a vertical axis wind turbine by comprehensive assessment of an airfoil family

Jian Chen[a], Liu Chen[a*], Hongtao Xu[a], Hongxing Yang[b] , Changwen Ye[b], Di Liu[b]

[a]School of Energy and Power Engineering, University of Shanghai for Science and Technology, Shang Hai, China

[b]Renewable Energy Research Group (RERG), The Hong Kong Polytechnic University, Kowloon, Hong Kong, China

E-mail: [a]chen_liu@usst.edu.cn

Studies on lift-type VAWTs are far fewer than those on horizontal VAWTS, especially in the field of airfoil, which is regarded as the fundamental of VAWT design. Existing researches seldom systematically and efficiently touch upon a specific airfoil family. Thus, a coupled approach comprising two steps was used in this paper to assess an airfoil family, wherein the first step was the orthogonal algorithm combined with an automatic computational fluid dynamic analysis (ACFDA) module, and the second step was the combination of the one-factor at a time (OFAAT) algorithm and the ACFDA module.

Results demonstrate that among three design parameters, the thickness-chord ratio (TCR) had the biggest effect on C_P while the maximum thickness in tenths of chord (MTITOC) had the smallest influence on C_P. By this approach, we found a desired airfoil having maximum power coefficient(C_{PMAX}) was 0.4585, app. 15.5% higher than that of the previously widely used rotor NACA 0015. In addition, detailed flow data (field) dispersing in the vicinity of the airfoil were visualized to reveal the effect of each design parameter on airfoil's aerodynamic behavior. Lastly,

this coupled approach can be used to assess any airfoil family that can be parameterized and has several design parameters.

Keywords: Airfoil assessment; Orthogonal algorithm; ACFDA module; Power coefficient (C_P); Impact weight; flow field

1. Introduction

According to International Energy Outlook 2011 (IEO 2011), world energy consumption will increase by 53% [1], from 505 quadrillion Btu in 2008 to 770 quadrillion Btu in 2035, as a result of robust economic growth and expanding populations in developing countries, especially when the demand for building services and comfort levels continues to increase in these countries. Moreover, energy consumptions in residential and commercial buildings in developed countries have increased by about 20% and 40% [2] respectively, far exceeding those in other major sectors (e.g. industry and transportation), not to mention the more and more restricted applications of traditional fossil fuel due to heavy environmental impact and declining reservoirs. The contradiction between the increasing demand of buildings for energy to meet both residential and commercial needs and the declining reservoir of fossil fuel tends to be more and more grave. So, the proposal of using clean and renewable energy in buildings is increasingly prevailing and acceptable to alleviate this contradiction.

Recently, an increasing interest has been aroused to harness wind energy in buildings by using smaller size wind turbines [3-6]. Lots of studies [7-9] show that the small vertical axis wind turbine (VAWT) seems to be a promising device to adapt to the complex wind environment in urban areas due to its appealing features, such as the independence of wind direction [10], low noise level [11], reduced sensitivity to the oncoming turbulent [12] and increasing energy output

in the skewed flow [13]. In the economic feasibility assessment of VAWT in urban environment conducted by D. Saeidi et al in 2013 [10], their VAWTs gained a profit of 6 cents per kWh based on 12 cents per kWh for renewable energy in Iran

There also emerges an interest of utilizing vertical axis wind turbines [14] to harness offshore wind resources. Thanks to the advantages such as lower center of gravity, reduced machine complexity and better scalability to very large sizes [15, 16], several multi-megawatt offshore Darrieus projects are currently underway.

2. Reviews of previous studies

However, airfoil researches on the VAWT are far fewer than those on the horizontal axis wind turbine (HAWT), especially on VAWT's airfoils. Most of the airfoil researches basically have two steps [17]. The first step is to decide an assessment or optimization algorithms, such as the pre-selected, OFAAT or differential evolution (DE) algorithm. And the second step is to predict the C_P of the rotor using the theoretical methods, such as the Momentum, Panel or computational fluid dynamic (CFD) method. Broadly speaking, the airfoil researches of VAWT have experienced three periods.

In the early period, airfoil researches largely involved in a limited numbers of airfoils from which abundant testing data could be collected. The reason why such data were needed is that the C_P prediction methods in this period were mostly the Momentum, Vortex and Cascade ones [18]. These C_P prediction methods require the availability of abundant experimental data in respect of lift coefficient (Cl), drag coefficient (Cd), and moment coefficient (Cm) over a wide range of angles of attack (AOA) and Reynolds numbers (RN). The Momentum, Vortex and Cascade methods are more robust and faster than the Panel or CFD method only when the reliability

66 characteristics of airfoils are well built or exist [19]. Thus, in this period, the preferred
67 assessment or optimization algorithm was mostly the OFAAT [20] or the pre-selected algorithm
68 [21, 22]. Airfoils evaluated were few and mainly came from the 4- [23] or 6-digital NACA series
69 [24], Gottingen series [25] and low Reynolds number series [26].

70 The second period began with the utilization of the Panel method to predict C_l, C_d and C_m of an
71 airfoil. In this period, several Panel-method-based codes (XFOIL [27], PROFIL [28]) were used
72 extensively to analyze the aerodynamic characteristics of airfoils before pre-stall [29]. Recently,
73 the Panel method has been introduced into some researches [30-32] to predict the C_P of
74 Darrieus rotor. However, because the potential theory, which ignores the viscosity of flow, is the
75 foundation of the Panel method, the effect of viscosity was introduced into these assessments
76 by way of some coupling models which are highly related to the external potential flow and the
77 inner viscous flow and are only capable of handling 'mild' separation [33]. For massive
78 separation, additional modeling efforts or the solution of full Navier-Stokes equations are
79 required. Thus, fewer airfoils were investigated in this period. Besides, the OFAAT or the pre-
80 selected algorithm was also the prevalent assessment or optimization algorithm in this period.

81 The third period began with the application of CFD method to predict the C_P of the Darrieus
82 rotor. For nearly a decade, the CFD method has been widely applied on the studies of VAWT due
83 to the fact that the CFD method can easily take into account the effects of dynamic stall,
84 viscosity, flow curvature and parasitic drag. Two airfoils (NACA 2415 camber and modified NACA
85 0018 airfoils) were compared by H. Beri [34], who employed the CFD method to examine the
86 self-starting ability. Three airfoils were considered by M.R. Castelli [35] in his study of the C_P of
87 the Darrieus rotor. Twenty pre-selected airfoils were assessed by Mohamed, MH [36], who
88 adopted the CFD method to study the C_P of Darrieus rotor. It is also noted that the assessment
89 or optimization algorithms used in those CFD studies were primarily based on the OFAAT or pre-

selected algorithm, while the OFAAT or pre-selected algorithm was unable to assess the impact of airfoil design parameters in a comprehensive manner. Thus, a few researchers have adopted advanced assessment or optimization algorithms to evaluate the airfoil using the CFD method. In 2012, Carrigan, T.J. [37] combined the differential evolution (DE) with the CFD method to study NACA 0018 airfoil for Darrieus rotor. By this coupled approach, the power output was increased by more than 6%. The DE algorithm in this case can be replaced with other similar algorithms, such as the evolutionary algorithm (EA), the genetic algorithm (GA) and the particle swarm optimization (PSO) algorithm. Nevertheless, it should be noted that DA, EA, GA and PSO algorithms are always hampered by high assessment cost and slow convergence [38] or swarm stagnation [39]. The computational cost is much greater in CFD method than in the Momentum, Vortex, Cascade method or the Panel method. Therefore, it will take many computational resources to conduct an airfoil optimal design or assessment by coupling the CFD method with the DA, EA, GA or PSO algorithm.

3. A novel coupled approach to assess the airfoil family

In this paper, a novel coupled approach was proposed to assess a specific airfoil family systematically and effectively. This coupled approach comprises two parts: an orthogonal algorithm is coupled with an automatic computational fluid dynamic analysis (ACFDA) module, and a OFAAT algorithm based on the orthogonal algorithm is coupled with an ACFDA module. The airfoil family investigated is the NACA 4-digital-modified airfoil family, an extension of the NACA 4-digital airfoil family that has three design parameters. This airfoil family is thought to have good stall characteristics.

The orthogonal algorithm that could efficiently evaluate the NACA 4-digital-modified airfoil family with minimum efforts was utilized to seek for optimization solutions. A comparison conducted by Tanaka. H [36] showed that the orthogonal algorithm could result in a solution to the same problems as GA could but with much less cost in computation. Another distinct advantage of the orthogonal algorithm, when compared with GA and EA algorithms, is that it can evaluate the impact weight of each design parameter. In this paper, the OFAAT algorithm was also applied for the assessment of the NACA 4-digital-modified airfoil family. Different from the conventional OFAAT algorithm, the OFAAT algorithm was used on the basis of conclusions gained from the orthogonal algorithm.

A homemade ACFDA module is created to accomplish the construction of computational domain, mesh generation, selection of CFD strategies and data analysis on its own effectively. It not only eliminates tedious mouse click operations but also cuts down a great deal of time cost thanks to the background operation of the software. Moreover, several CFD strategies were discussed to save the computational time.

This coupled approach can be applied to assess airfoil families or series that can be parameterized. With the development of aviation and turbo machinery industry, lots of functions [37] and mathematical tools [38, 39] are available for researchers to describe the geometry of airfoils. By applying these functions and tools, the programming language can help to obtain detailed cross-section data on airfoils, and files that contain and reflect the geometry information can be introduced into the above-mentioned ACFDA module and then evaluated by the orthogonal algorithm.

4. Description of the NACA 4-digit-modified airfoil family and the H-Darrieus rotor

Many airfoil assessment researches focus on NACA 4-digit airfoil families that have just one design parameter. So the OFAAT algorithm is enough to assess this airfoil family. But this algorithm will no longer be suitable when the airfoil family has more than one design parameters, like the NACA 4-digit-modified airfoil family which has three design parameters (i.e. thickness-chord ratio (TCR), leading-edge radius(LEN) and Maximum thickness in tenths of chord (MTITOC)). The designation of NACA 4-digit-modified airfoil family is a NACA 4-digit followed by a dash and then a 2-digit number. For example, in the case of NACA 0015-63, the first four digits means that the airfoil belongs to a 4-digit airfoil family, of which the first two digits, i.e. 00, indicate it is a symmetrical airfoil and the following two digits represents TCR; and in the last two digits following the dash sign, the first digit is a leading-edge index and the second digit represents the location of MTITOC aft of the leading edge.

Equations of NACA 4-modified-digit airfoil family are described below [40]:

For ordinates from leading edge to maximum thickness:

$$\frac{y}{c} = a_0(\frac{X}{c})^{1/2} + a_1(\frac{X}{c}) + a_2(\frac{X}{c})^2 + a_3(\frac{X}{c})^3 \quad (1)$$

For ordinates from the maximum thickness to trailing edge:

$$\frac{y}{c} = d_0 + d_1(1 - \frac{X}{c}) + d_2(1 - \frac{X}{c})^2 + d_3(1 - \frac{X}{c})^3 \quad (2)$$

The constants ($a_0, a_1, a_2, a_3, d_0, d_1, d_2, d_3$) in above equations for t/c =0.2 were calculated from the following boundary conditions:

Maximum ordinate:

$$\frac{x}{c} = m \qquad \frac{y}{c} = 0.1 \qquad \frac{dy}{dx} = 0 \tag{3}$$

Leading-edge radius:

$$\frac{x}{c} = 0 \qquad R = \frac{a_0^2}{2} \tag{4}$$

Radius of curvature at maximum thickness:

$$\frac{x}{c} = m \qquad R = \frac{(1-m)^2}{2d_1(1-m) - 0.588} \tag{5}$$

Ordinate at trailing edge:

$$\frac{x}{c} = 1.0 \qquad \frac{y}{c} = d_0 = 0.002 \tag{6}$$

Magnitude of trailing-edge angle:

$$\frac{x}{c} = 1.0 \qquad \frac{dy}{dx} = d_1 = f(m) \tag{7}$$

where c is the chord length, t is the thickness of the airfoil.

Table 1 Relationship between values of d_1 and values of m

Table 2 Relationship between leading-edge index number and values of a_0

d_1 values were chosen on the basis of studies conducted by Stack, J and Von Doenhoff, A.E. [41] in order to avoid curvature reversal. Table 1 gives the relationship between d_1-value and m-value, and the leading-edge index is proportional to a_0, as indicated in Table 2. Depending on

above equations, the code compiled with MATLAB programming language will generate the ordination of NACA 4-modified-digit-series airfoils. This ordination of airfoils is the input file of the ACFDA module mentioned in the Methodology Section. The radius of the Darrieus rotor with three blades was 1.25m; the chord length of the airfoil was 0.25m; the central point of the installed struts was one quarter of the chord length; and the height of H-Darrieus was 3.75m.

5. Methodology

As stated in the Introduction Section, this assessment approach comprises two steps:

Step1: Orthogonal algorithm + ACFDA module; and

Step2: OFAAT algorithm based on the results gained from Step 1+ ACFDA module

The aim of Step1 is to assess the impact factor of each design parameter in a systematized manner. This step may possibly lead to an optimal combination of design parameters. The OFAAT algorithm based on the results gained from step1 is adopted in Step2 for further study. In fact, the core part of this assessment approach is the orthogonal algorithm and the ACFDA module. Hence, a brief introduction about the orthogonal algorithm and the ACFDA module will be presented in the following paragraphs.

5.1 Orthogonal algorithm

At the heart of the orthogonal algorithm is the orthogonal array which will lead to a solution with minimum efforts. The array can be expressed as $L_n(x^y)$, where n is the No. of rows in the array, x is the No. of levels in the columns, and y is the No. of columns in the array.

As the NACA 4-modified-digit airfoil family has three design parameters, these design parameters became the factors of the orthogonal array in this paper, and the value of each parameter was considered as the level of the orthogonal array.

Table 3 Investigated factors and levels

A full factorial investigation can help to reveal the effect of all factor combinations on C_P, but it will take great efforts to conduct such an investigation. For instance, there are 64 different combinations to be evaluated if the case in question has three factors and each factor has four levels. As one combination takes about 28 hours to obtain the C_P curve with 8 points (Processor--Intel(R) Core(TM) i5-4570 CPU @ 3.20GHz 3.20GHz, RAM--8GB), it will take 1792 hours or roughly 2.49 months to complete the full factorial investigation for 64 combinations. For comparison, the orthogonal array requires only 16 combinations if it has three factors and each factor has four levels. This time-saving property of the orthogonal array can quite well compensate for the time consumption drawback of the CFD simulation.

Table 4 Orthogonal list $L_{16}(4^5)$

In order to maintain the equivalence property of the orthogonal array [42], the levels of each design parameter were selected isotropically. The TCR of airfoil ranged from 0.15 to 0.24; the LEN ranged from 0 to 9; and the MTITOC aft of the leading edge ranged from 2 to 5. The smallest value of TCR was 0.15, as TCR=0.12 was too small considering the structure issue mentioned by Migliore et al. [20]. Table 3 presents the levels and factors studied in this paper.

The orthogonal list $L_{16}(4^5)$, as displayed in Table 4 was used for experiments involving less than four levels and five factors. The three factors and four levels were investigated for the NACA 4-modified airfoil family. The last two columns were not necessary because three factors

209 were considered. The levels of each factor for the airfoil are bracketed in Table 4. Therefore 16
210 combinations (i.e. 16 different airfoils) were investigated, which were NACA 0015-02, NACA
211 0015-33, NACA 0015-64, NACA 0015-95, NACA 0018-03, NACA 0018-32, NACA 0018-65, NACA
212 0018-94, NACA 0021-04, NACA 0021-35, NACA 0021-62, NACA 0021-93, NACA 0024-05, NACA
213 0024-34, NACA 0024-63 and NACA 0024-92 respectively. The MATLAB program generated
214 airfoils' geometry data files based on equations specified in Section 2 and passed those files to
215 the ACFDA module discussed in Section 3.2.

216 5.2 The automatic CFD analysis process

217 The ACFDA module, showed in Figure 1, consists of four procedures, the airfoil geometry
218 generation procedure, the mesh generation procedure, the CFD simulation procedure, and the
219 results analysis procedure. Each procedure has a function program that can be used to create
220 files needed in the subsequent procedure. As discussed in Section 2, the MATLAB program
221 creates several airfoil geometry files using the equations in section 3 firstly. Secondly, the
222 MATLAB program calls the Gambit program in batch mode controlled by the Gambit's journal
223 code to read the airfoil geometry files and generate the mesh file of the computational domain
224 automatically. Then, the MATLAB program will call the FLUENT program controlled by the
225 FLUENT's journal code to select the CFD strategies and export the CT files of the rotor. And the
226 MATLAB program will process the C_T files to attain the C_P of rotor. The MATLAB program
227 organizes four procedures of the ACFDA module in a sequential way in which the specified code
228 or journal file executes related function programs all on its own not only to eliminate tedious
229 simulation operations but also cut down a great deal of time cost owing to the background
230 operation of the software.

Figure 1 Orthogonal algorithm and ACFDA module

6. CFD strategies and validation of the simulation results

6.1 Discussion on CFD strategies

Table 5 A detailed summary of the CFD simulation on VAWTs (1)

Table 6 A detailed summary of the CFD simulation on VAWTs (2)

The reliability of CFD simulation is crucial to the entire assessment process. Based on author's review (Table 5 and Table 6), a two-dimensional computational domain was constructed by using the most popular CFD strategies in order to validate the simulation results. This 2D computational domain is displayed in Figure 2, which also exhibits a detailed mesh enveloping the airfoil surface. In the assessment, the ANSYS FLUENT code was employed to predict the C_P of rotors; the governing equations were discretized by the finite volume method; the solver was the pressure-velocity based segregated solver; the first-order implicit scheme was used for time integration; the SIMPLE [43-45] algorithm coupled the pressure and velocity; and the second-order interpolation scheme [46, 47] was chosen for the pressure and momentum equation.

Considering the unsteady time-periodic motion of the rotor, the sliding mesh technique adopted allows the adjacent grid to slide relative to one another. The inlet was the velocity inlet and the outlet was the pressure outlet. The SST $\kappa-\omega$ [48-50] turbulence model was used to take into account the flow nature of adverse pressure gradients and boundary layer separation for a rotating Darreius rotor. The Y plus value ranged from 0 to 1.7 [48, 51] to properly resolve the viscous sub layer. The convergence criteria were designed in such a manner as to satisfy the maximum residue of 1.0x10-5 and to get a periodical torque variation. Most of the CFD

252 strategies were identified based on Table 5 and Table 6. Also in this paper, the computational
253 domain size, time step size and rotational turns were discussed to reduce the computational
254 cost.

255 The computational domain was a square shape, so the side length of the square was the only
256 parameter of the computational domain. The computational domain ratio was defined as the
257 ratio of the side length of the square to the diameter of the rotor. Figure 3 shows the effect of
258 this ratio on C_P. In this paper, five different ratios (i.e. 10, 15, 20, 25 and 30) were compared.
259 Theoretically, the smaller the computational domain is, the less the mesh number will be. From
260 this figure, it is obvious that the C_P of rotor is relatively stable when the computational domain
261 ratio is larger than 15. Thus, the computational domain is fifteen times larger than the diameter
262 of the rotor. A comparison was further conducted between cases having different total mesh
263 numbers (about 0.4, 0.6 and 0.8 million). As the difference between simulated C_T values of these
264 three cases was negligible, the 0.4-million mesh number was used in the case of having 15
265 computational domain ratios. In general, larger time steps means lower computational cost, so
266 it is advantageous to set the size of the time step as large as possible. However, a larger time-
267 step size may result in non-convergence. Because of this, three time-step sizes were
268 investigated in this paper. In a study conducted by McLaren, K.W [52] , five different time-step
269 sizes, which were 0.5, 1, 2.5, 5 and 10 degrees respectively at each time step, were discussed
270 and it was found that C_T curves of 0.5, 1 and 2.5 degrees were close to each other at each time
271 step. Significant improvements were also noted in C_T curves when the number of degrees at
272 each time step was larger than 5. Considering the time-saving benefit and when allowing the
273 flow variable to adjust in an appropriate manner, 2.5 degrees at each time step was selected in
274 this paper.

Figure 2 Schematic of computational domain

Another influencing factor is the number of turns, which is critical as it can remarkably affect the accuracy and computational cost. Generally speaking, the larger the number of turns is, the more stable and accurate the results will be. However, larger numbers of turns more than often mean the input of greater computational efforts. So a trade-off between the accuracy and the computational cost is required for the selection of proper number of turns. Figure 4 displays the C_T curve that varies with the number of turns. A slight variation is found in CT curves when the number of turns exceeds 5. So 5 turns were selected for simulated rotors in this paper. Using the selected CFD strategies mentioned above, each TSR took about 3.5 hours to finalize the calculation. Considering the fact that eight TSR values were chosen for each C_P or CT curve, 28 hours were necessary in order to build the C_P or C_T curve of a rotor with the assigned airfoil.

Figure 3 Computational domain ratio

Figure 4 Number of turns

6.2 Validation of the CFD simulation with experimental results

In order to validate the reliability of the selected CFD strategies, a simulation model was built according to the rotor tested by Fiedler [53]. Figure 5 shows the comparison between the simulated results and the experimental results. It can be observed that the simulated results match well with the experimental results when the TSR is less than 1.5. Overestimation of C_P is detected when TSR is larger than 1.5. This overestimation of C_P at a higher tip speed ratio was also illustrated by Mclaren, K.M [52]. The validation results gained in this paper were fairly similar to the results gained by Almohammadi. K.M [44], who conducted a CFD mesh independent study for a vertical axis wind turbine. Several reasons may account for this

297 divergence, including the geometrical mismatch between the 2D simulated and 3D tested rotors,
298 the selection of CFD strategies, and so on. However, it is important to note that the location of
299 the simulated C_{PMAX} is the same as the experimental results, and the variation tendency of the
300 simulated results is comparable to that of the experimental results.

301 Figure 5 Validation of the simulated results

302 6.3 Validation of the results with conclusion from the NACA 4-digital
303 airfoil family

304 TCR is the sole design parameter related to the NACA 4-digit airfoil family. So the effect of TCR
305 on rotor performance was studied through this ACFDA module in order to qualitatively validate
306 the prediction ability of the CFD simulation. The studied TCRs, which were 0.15, 0.18, 0.21 and
307 0.24, are displayed in Figure 6.

308 The simulated results are shown in Figure 7, from which it is evident that the value of C_{PMAX}, as
309 well as the value of C_{TMAX}, of the rotor increases as the TCR decreases and the C_P curve even
310 reaches the highest at 0.41805 (i.e. $C_{PMAX=}$0.41805) for the rotor with NACA 0015. This
311 conclusion is similar to the that gained by Miglioreet al. [20]. Hence, these simulation results
312 again qualitatively validate the prediction ability of the determined CFD strategies.

313 Figure 6 Four NACA 4-digital airfoils with different TCRs

314 Figure 7 Effect of the TCR on the performance of the rotor (NACA 4-digital airfoil family)

315 7. Results

7.1 Orthogonal algorithm and ACFDA module for NACA 4-digital-modified airfoil family

Drawings of 16 NACA 4-digital-modified airfoils gained from the orthogonal array are presented in Figure 8. From the top down, the TCR increases from 0.15 to 0.21. Those airfoil data were imported to the ACFDA module to gain C_P curves of rotors at eight different TSRs, which are illustrated in Figure 9. The simulation results are shown in Figure 9. It is found that the C_P curve reaches the highest and lowest respectively for rotors with NACA 0015-64 airfoil and NACA 0024-93 airfoil, especially when the TSR range is larger than 2. C_{PMAX} values generally range from 0.3 to 0.42 for most rotors, and the working TSR range of these rotors is mainly larger than 4, except for the rotor with NACA 0024-93 airfoil. It must be emphasized that the TSR value of C_{PMAX} is not a constant, although it fluctuates around 2.5 for most rotors. This value varies as the airfoil design parameters differ when other design parameters of the rotor are fixed, indicating that the TSR value of C_{PMAX} cannot be predetermined in the first place when a C_P assessment is made on the airfoil.

The impact of each design parameter on C_{PMAX} is discussed in Table 7. As can be noted, the 1st through the 16th rows and the 1st through the 3rd columns of Table 7 are the same with the corresponding rows and columns of Table 4. The final column of Table 7 lists the C_{PMAX} of each corresponding case. K_1 includes three numbers: the first number represents the sum of C_{PMAX} for airfoils which have the factor A at level 1 in the first column; the second number is the sum of C_{PMAX} for rotors which have the factor B at level 1 in the second column; and the third number is the sum of C_{PMAX} for rotors which have the factor C at level 1 in the third column. Calculations of these three numbers of K_2 is the same as K_1. The only difference is that K_2 is the sum of C_{PMAX} at level 2 for each column.

Figure 8 Sixteen NACA 4-digital-modified airfoils for the orthogonal algorithm

Figure 9 Power curves of sixteen NACA 4-digital-modified airfoils

Table 7 The C_{PMAX} results of the orthogonal method for 16 NACA 4-digital-modified airfoils

Table 7 The C_{PMAX} results of the orthogonal method for 16 NACA 4-digital-modified airfoils (continued)

The first number of K_1' is the average of C_{PMAX} for airfoils which have the factor A at level 1 in the first column. The difference between K_1' and K_1 is that K_1 is the sum of C_{PMAX} while K_1' is the average of C_{PMAX}.

The difference between max(K_i') and min(K_i') is listed in the final row of Table 7. This difference reveals the impact weight of different factors. The last row of Table 7 provides the optimum level for different factors.

Based on the above analysis, the optimal level of factor A, factor B and factor C was 1, 3 and 3 respectively and the airfoil corresponding to the optimal level was a NACA 0015-64 airfoil. This optimal airfoil was one of the airfoils tested. It is known from the comparison of C_{PMAX} between 16 cases exhibited in Table 7 that the rotor with NACA 0015-64 had the best C_P, which was 0.413975. It is also found that among the impact weights of three factors, the TCR ranked first, the LEN came second, and the MTITOC had the smallest impact on the power coefficient. It should be noted that the C_{PMAX} gained by orthogonal algorithm was slightly smaller than that of the NACA 0015 airfoil (Section 4.3) owing to the evaluation in the partial domain. However, the orthogonal algorithm did offer the impact weight of each design parameter. Therefore, a further study was performed by using the OFFAT algorithm and ACFDA module based on the conclusions gained from the orthogonal algorithm.

7.2 OFAAT algorithm based on orthogonal algorithm and ACFDA module for NACA 4-digital-modified airfoil family

Figure 10 Twelve NACA 4-digital-modified airfoils studied by OFAAT algorithm

This part will discuss the coupling of OFAAT algorithm and CFD module on the basis of conclusions gained from the orthogonal algorithm. Three groups of assessments have been carried out to clarify the effect of each factor and to extend the orthogonal algorithm.

In the assessment of changes of MTITOC, TCR was 0.15 and LEN was 6. Hence, four airfoils (i.e. NACA 0015-62, NACA 0015-63, NACA 0015-64, and NACA 0015-65) were studied for this assessment.

In the assessment of changes of LEN, TCR was 0.15 and MTITOC was 4. Four airfoils (i.e. NACA 0015-04, NACA 0015-34, NACA 0015-64, and NACA 0015-94) were investigated for this assessment.

In the end, the effect of TCR was studied when LEN was 6 and MTITOC was 4. Four airfoils (i.e. NACA 0015-64, NACA 0018-64, NACA 0021-64, and NACA 0021-64) were examined for this assessment. Figure 10 depicts the airfoils which were studied by OFAAT algorithm based on the orthogonal algorithm.

7.2.1 MTITOC for NACA 4-digital-modified airfoil family

Figure 11 The effect of the MTITOC on C_P (NACA 4-digital-modified airfoil)

Table 8 Maximum and average C_P for MTITOC (NACA 4-digital-modifed airfoil)

The effect of MTITOC on C_P is given in Figure 11. From this figure, it is evident that the highest C_{PMAX} does not occur for the rotor with NACA 0015-64, which is the best candidate for the assessment of orthogonal method; that the best C_{PMAX} in the assessment of OFAAT algorithm is 0.41655 for the rotor with NACA 0015-62 airfoil; and that the rotor with NACA 0015-65 has the lowest C_{PMAX}. Table 8 shows the average C_P of rotor at different TSRs. It should be noted that the varying pattern of C_{PMAX} is quite similar to that of the average C_P. So the best airfoil can also be determined by comparing average C_P.

It should be also noted that the orthogonal method is a statistical method adopted to find solutions with minimum efforts. For this purpose, the orthogonal method considered several combinations of the whole solution space. It is not surprising that the best candidate of the orthogonal algorithm may not be the best candidate of the OFAAT algorithm. To put it in another way, the orthogonal method did offer valuable guidance for airfoil assessment because the C_P difference between rotors evaluated by OFAAT algorithm was quite small. This small difference conformed to the conclusion gained from the orthogonal algorithm, which indicated that the impact weight of MTITOC was the smallest. So according to results from the OFAAT algorithm, this OFAAT algorithm assessment was worthy of conducting. In the end, the C_{PMAX} didn't vary linearly with the MTITOC when TCR was 0.15 and LEN was 6.

This small difference mainly occurred at the azimuth angle ranging from 90° to 180° (as showed in Figure 12). The curves of instantaneous C_T for four different rotors were close to each other in the downstream zone. Figure 13 and Figure 14 illuminate the instantaneous contour of total pressure and streamline for blade No.1 at TSR=2.5 at eight different azimuth angles. From these figures, it is found that an obvious vortex is formed at the inner side of the airfoil surface for four airfoils when the azimuth angle is 135°, and this separation area increases with the increasing of MTITOC; that this separation is found for NACA 0015-63, NACA 0015-64 and NACA

0015-65 airfoils at azimuth angle 180° but vanishes for NACA 0015-62 airfoil at the same angle; and that this vortex even lasts until the azimuth angel reaches for NACA 0015-65 airfoil. This might be the probable reason why C_{PMAX} values of NACA 0015-62 and NACA 0015-65 are respectively the highest and the lowest. Overall, larger MTITOCs generate larger vortexes on the airfoil inner surface almost throughout the whole azimuth angle range.

Figure 12 Instantaneous C_T of blade #1 as a function of azimuth angle (MTITOC)

Figure 13 Instantaneous contours of pressure coefficient and streamline for blade No.1 at TSR=2.5 in upwind zone (MTITOC)

Figure 14 Instantaneous contours of pressure coefficient and streamline for blade No.1 at TSR=2.5 in downwind zone (MTITOC)

7.2.2 The LEN for NACA 4-digital-modified airfoil family

Figure 15 The effect of the LEN (NACA 4-digital-modified airfoil)

Figure 16 Instantaneous C_T as a function of azimuth angle (LEN)

Figure 15 presents the effects of LEN on C_P and C_T. Obviously, with the increasing of LEN, the C_P curve first increases and then declines. The best airfoil (NACA 0015-64) of the orthogonal algorithm is the best one for this OFAAT algorithm assessment. In addition, the C_P curve of the rotor with zero LEN is extremely lower than that of other rotors. Therefore, small LENs should be avoided when a selection is taken in the NACA four-digital-modified airfoil family. The C_P difference between rotors with NACA 0015-64 and NACA 0015-94 is not very large, suggesting that the airfoil with large LEN had a better C_P, especially when this number is greater than 6. The TSR of the optimal C_P is 2.5 for most of the rotors. The effect of LEN on C_T is equal to the LEN on C_P.

Instantaneous C_T curves in Figure 16 show that the main difference among four airfoils is located within the azimuth angle ranging from 50° to 170°. Instantaneous C_T values of NACA 0015-04 are smaller than those of other airfoils in almost the whole azimuth angle range. The reason for this can be found in Figure 17 and Figure 18. For NACA 0015-04, a leading edge vortex appears first on the inner surface at azimuth angle 90°. Then, a new vortex develops in the middle of the inner surface at azimuth angle 135°. At azimuth angle 180°, two vortexes are merged to form a large leading edge vortex. As the azimuth angle further increases, this large leading edge vortex moves to the trailing edge of the airfoil. For NACA 0015-34, a large leading edge vortex grows at azimuth angle 135° and vanishes at azimuth angle 315°. However, the vortex on the inner surface is very small for NACA 0015-64 and NACA 0015-94 airfoils and can only be found at azimuth angles 135° and 180°. Hence, the airfoil with small LEN forms a larger leading edge vortex than the one with large LEN

Figure 17 Instantaneous contours of pressure coefficient and streamline for blade No.1 at TSR=2.5 in upwind zone (LEN)

Figure 18 Instantaneous contours of pressure coefficient and streamline for blade No.1 at TSR=2.5 in downwind zone (LEN)

In the orthogonal algorithm, LEN is the second important influential factor. By comparing rotors with zero LEN and no-zero LENs, a large difference is revealed. This difference decreases when the leading edge number is larger than 3, indicating that the influencing ability of LEN mainly comes from the zero LEN. This C_P difference found in Figure 15 again proves the reliability of the conclusion gained from the orthogonal algorithm.

7.2.3 TCR for NACA 4-digital-modified airfoil family

Unlike the thickness chord ratio effect in Section 4.3, it is found in Figure 19 that with the increasing of TCR, the C_P first increases and then decreases. So the C_P of the rotor is not purely dependent on the TCR of airfoil. All three design parameters will have a joint impact on C_P. The conclusion gained from NACA 4-digit airfoil family is only suitable when MTITOC is 0.3 and the leading-edge radius varies as the square of the TCR.

Figure 19 The effect of TCR (NACA 4-digital-modified airfoil)

Figure 19 displays a very notable discovery: the C_P of rotor with NACA 0018-64 airfoil is much higher than that of other rotors, especially when TSR is larger than 2. Till now, it is clear that the TSR of optimal C_P for the majority of rotors was 2.5. However, the TSR of optimal C_P for rotor with NACA 0018-64 airfoil was 3, which was slightly larger than that of other rotors. This higher TSR of optimal C_P not only reduces the transient variation of AOA, but also weakens the occurrence of the dynamic stall. The extended TSR range also enhances the ability of the steady power output. In addition, it is noteworthy that the optimal TSR cannot be fixed at a constant TSR when conducting an airfoil assessment research, as it will leave out the optimal airfoil whose TSR of optimal C_P is not this constant TSR value.

As discussed in the orthogonal algorithm, the TCR had the greatest impact on rotors' C_P values. The C_P difference among four rotors found in Figure 19, especially when TSR>2, was consistent with the above conclusion.

Figure 20, Figure 21 and Figure 22 present the instantaneous C_T, pressure contour and streamline for blade No.1 in the entire azimuth angle range. As known from Figure 20, the large difference happened within the 50° ~ 180° azimuth angle range, whose conclusion is

supported by Figure 21 and Figure 22. Moreover, vortexes were found at azimuth angles 135° and 180° for four airfoils. At azimuth angle 135°, vortexes of airfoils with TCR=15 and TCR=18 appeared to attach to the inner surface of the airfoil. Vortexes of airfoils with TCR=21 and TCR=24 left the airfoil's inner surface and moved to the trailing edge, indicating that vortexes of airfoils with TCR=21 and TCR=24 were formed within the 90° ~ 135° azimuth angle range. At azimuth angle 180°, vortexes of airfoils with TCR=15 and TCR=18 remained attached to the inner surface of the airfoil. However, new vortexs were formed for airfoils with TCR=21 and TCR=24. At azimuth angle 225°, the inner vortex vanished for the airfoil with TCR=15. At azimuth angle 270°, inner vortexes re-emerged on the surface of four airfoils and appeared to be fairly smaller than inner vortexes formed at azimuth angles 135° and 180°. An interesting finding at azimuth angle 315° is that a very small vortex occurred on the outer surface for airfoils with TCR=18 and TCR=24. Generally speaking, the size and occurrence of vortexes generated on the airfoil NACA 0018-64 was the smallest and least possible in this airfoil group

Figure 20 Instantaneous C_T as a function of azimuth angle (TCR)

Figure 21 Instantaneous contour of pressure coefficient and streamline for blade No.1 at TSR=2.5 in upwind zone (TCR)

Figure 22 Instantaneous contour of pressure coefficient and streamline for blade No.1 at TSR=2.5 in downwind zone (TCR)

As a whole, the optimal airfoil series to be selected in the NACA 4-digit airfoil family was NACA 0015; the optimal rotor in the orthogonal algorithm was the rotor with NACA 0015-64 airfoil; the optimal rotor in the MTITOC-based OFAAT algorithm was the rotor with NACA 0015-62 airfoil; the optimal rotor in the LEN-based OFFAT algorithm was the rotor with NACA 0015-64 airfoil; the optimal rotor in the TCR-based OFAAT algorithm was the rotor with NACA 0018-64; the

492 C_{PMAX} values of rotors with NACA 0015, NACA 0015-62 and NACA 0015-64 were 0.41805,
493 0.41655 and 0.41075 respectively; and the C_{PMAX} of rotor with NACA 0018-64 was 0.4585, which
494 was app. 15.5% higher than that of the rotor with NACA 0015. Thus, this assessment approach
495 by combining the OFAAT algorithm with the orthogonal algorithm and ACFDA module found an
496 optimal airfoil for Darreius rotor from the NACA 4-digital-modified airfoil family. In addition, this
497 coupled approach is also capable of efficiently and systematically evaluating the effect of design
498 parameters.

499 8. Summary and conclusion

500 The aim of this paper was to develop a methodology to effectively assess an airfoil family in a
501 systematical manner by coupling the orthogonal algorithm and OFAAT algorithm with the
502 ACFDA module. The evaluated airfoil family was the NACA 4-digit-modified airfoil family. 25
503 airfoils were accessed in this paper. The following is a brief summary of conclusions obtained
504 from this assessment:

505 The orthogonal and OFAAT algorithms was integrated with the ACFDA module to create a two-
506 step airfoil assessment approach. In the first step, the impact weight of design parameters was
507 revealed and the results show that TCR has the biggest effect on C_P and MTITOC has the smallest
508 impact on C_P, which offers the theoretical guidance for the design of an airfoil.

509 For the second step, the conclusions gained from the OFAAT algorithm comply with those
510 gained from the orthogonal algorithm. To gain a higher C_P, smaller MTITOCs are preferred when
511 other design parameters remain unchanged. A larger MTITOC will generate larger vortexes on
512 the airfoil inner surface almost throughout the whole azimuth angle range. Identically, larger
513 LENs are preferred when the other two design parameters are fixed due to the mild leading-

edge separation. However, it is found that the C_{PMAX} will no longer increase when TCR reduces and the optimal TCR appears to be 18 when the MTITOC is 4 and TOC is 6.

An optimal airfoil (NACA 0018-64) is found when the OFAAT algorithm is conducted for TCR. The C_{PMAX} of rotor with NACA 0018-64 is 0.4585, app. 15.5% higher than that of the rotor with NACA 0015.

There is also a very important discovery that the optimal TSR of rotor varies with the design parameters of the airfoil. Thus, it is important to note that the optimal TSR cannot be fixed at a constant TSR in the airfoil assessment research.

In the end, this systematic and efficient assessment approach can be used to assess any airfoil family which has several design parameters.

Acknowledgments

The work outlined in this paper was supported by the Shanghai Pujiang Program (No. 15PJ1406200) and Shanghai Outstanding Talents Support Program (No.5113301101). Appreciation is also given to the Dean Reserve funding of The Hong Kong Polytechnic University (1-ZV3W).

9. Reference

1. Conti, J. and P. Holtberg, *The International Energy Outlook 2011*. 2011, U.S. Energy Information Administration: Washington, DC. p. 301.
2. Perez-Lombard, L., J. Ortiz, and C. Pout, *A review on buildings energy consumption information.* Energy and Buildings, 2008. **40**(3): p. 394-398.
3. Lu, L. and K.Y. Ip, *Investigation on the feasibility and enhancement methods of wind power utilization in high-rise buildings of Hong Kong.* Renewable and Sustainable Energy Reviews, 2009. **13**(2): p. 450-461.

4. Watson, J., et al., *Domestic micro-generation: Economic, regulatory and policy issues for the UK.* Energy Policy, 2008. **36**(8): p. 3095-3106.

5. Peacock, A.D., et al., *Micro wind turbines in the UK domestic sector.* Energy and Buildings, 2008. **40**(7): p. 1324-1333.

6. Allen, S.R., G.P. Hammond, and M.C. McManus, *Prospects for and barriers to domestic micro-generation: A United Kingdom perspective.* Applied Energy, 2008. **85**(6): p. 528-544.

7. Balduzzi, F., et al., *Feasibility analysis of a Darrieus vertical-axis wind turbine installation in the rooftop of a building.* Applied Energy, 2011(0).

8. Islam, M., D.S.K. Ting, and A. Fartaj, *Assessment of the small‐capacity straight‐bladed VAWT for sustainable development of Canada.* International journal of environmental studies, 2007. **64**(4): p. 489-500.

9. MARUYAMA, Y., et al. *Development of Vertical Axis Wind Turbine with Straight Blades Suitable for Buildings*. in *Proceedings of the European Wind Energy Conference*. 2001. Copenhagen, Denmark.

10. Saeidi, D., et al., *Aerodynamic design and economical evaluation of site specific small vertical axis wind turbines.* Applied Energy, 2012.

11. Aslam Bhutta, M.M., et al., *Vertical axis wind turbine–A review of various configurations and design techniques.* Renewable and Sustainable Energy Reviews, 2012. **16**(4): p. 1926-1939.

12. Balduzzi, F., et al., *Feasibility analysis of a Darrieus vertical-axis wind turbine installation in the rooftop of a building.* Applied Energy, 2012. **97**: p. 921-929.

13. Mertens, S., G. van Kuik, and G. van Bussel, *Performance of an H-Darrieus in the skewed flow on a roof.* Journal of solar energy engineering, 2003. **125**: p. 433.

14. Tjiu, W., et al., *Darrieus vertical axis wind turbine for power generation I: Assessment of Darrieus VAWT configurations.* Renewable Energy, 2015. **75**: p. 50-67.

15. Kim, S. and C. Cheong, *Development of low-noise drag-type vertical wind turbines*, in *Renewable Energy*.

16. Sargolzaei, J. and A. Kianifar, *Neuro–fuzzy modeling tools for estimation of torque in Savonius rotor wind turbine*, in *Advances in Engineering Software*. 2010. p. 619-626.

17. Koziel, S. and X.-S. Yang, *Studies in Computational Intelligence-Computational Optimization Methods and Algorithms*, ed. S. Koziel. 2011, Verlag Berlin Heidelberg: Springer.

18. Islam, M., D.S.K. Ting, and A. Fartaj, *Aerodynamic models for Darrieus-type straight-bladed vertical axis wind turbines.* Renewable and Sustainable Energy Reviews, 2008. **12**(4): p. 1087-1109.

19. Wang, Y.-F. and M.-S. Zhan, *3-Dimensional CFD simulation and analysis on performance of a micro-wind turbine resembling lotus in shape*, in *Energy and Buildings*. 2013. p. 66-74.

20. Migliore, P. and J. Fritschen, *Darrieus wind-turbine airfoil configurations.* NASA STI/Recon Technical Report N, 1982. **83**: p. 21600.

21. Zervos, A., *Aerodynamic Evaluation of Blade Profile for Vertical Axis Wind Turbines.*, in *European Wind Energy Conference* 1988: Herning, Denmark. p. 611-616.

22. Zervos, A., *Aerodynamic Design of Blade Profiles for Vertical Axis Wind Turbines*, in *Euroforum, New Energies*. 1988: Saarbrücken, F.R. Germany. p. 24-28.

23. Migliore, P.G., *Comparison of Naca 6-Series and 4-Digit Airfoils for Darrieus Wind Turbines.* Journal of Energy, 1983. **7**(4): p. 291-292.

24. Claessens, M., *The design and testing of airfoils for application in small vertical axis wind turbines.* Master of Science Thesis, 2006.

25. Baker, J., *Features to aid or enable self starting of fixed pitch low solidity vertical axis wind turbines.* Journal of Wind Engineering and Industrial Aerodynamics, 1983. **15**(1): p. 369-380.

26. Klimas, P.C., *Airfoil treatments for vertical axis wind turbines*, in *WINDPOWER `85*. 1985: San Francisco, CA, USA.

27. Drela, M., *XFOIL: An analysis and design system for low Reynolds number airfoils*, in *Low Reynolds number aerodynamics*. 1989, Springer. p. 1-12.

28. Knüppel, O., *PROFIL/BIAS—a fast interval library.* Computing, 1994. **53**(3-4): p. 277-287.

29. Somers., D.M. and M.D. Maughmer., *Theoretical Aerodynamic Analyses of Six Airfoils for Use on Small Wind Turbines*. 2003, National Renewable Energy Laboratory: Colorado.

30. Wang, L., L. Zhang, and N. Zeng, *A potential flow 2-D vortex panel model: Applications to vertical axis straight blade tidal turbine.* Energy Conversion and Management, 2007. **48**(2): p. 454-461.

31. Simão Ferreira, C., *The near wake of the VAWT: 2D and 3D views of the VAWT aerodynamics*. 2009, PhD Thesis, Technische Universiteit Delft, The Netherlands.

32. Dixon, K., *The Near Wake Structure of a vertical axis wind turbine-Including the Development of a 3D Unsteady Free-Wake Panel Method for VAWTs*, in *Faculty of Aerospace Engineering*. 2008, Delft University of Technology.

33. Katz, J. and A. Plotkin, *Low-speed aerodynamics*. Vol. 13. 2001: Cambridge University Press.

34. Beri, H. and Y. Yao, *Numerical Simulation of Unsteady Flow to Show Self-starting of Vertical Axis Wind Turbine Using Fluent.* Journal of Applied Sciences, 2011. **11**: p. 962-970.

35. Castelli, M.R., G. Simioni, and E. Benini, *Numerical Analysis of the Influence of Airfoil Asymmetry on VAWT Performance*, in *World Academy of Science, Engineering and Technology 61*. 2012. p. 312-321.

36. Mohamed, M., *Performance investigation of H-rotor Darrieus turbine with new airfoil shapes.* Energy, 2012.

37. Carrigan, T.J., et al., *Aerodynamic Shape Optimization of a Vertical-Axis Wind Turbine Using Differential Evolution.* ISRN Renewable Energy, 2012. **2012**.

38. Kwon, Y.-D., et al., *Convergence enhanced genetic algorithm with successive zooming method for solving continuous optimization problems.* Computers & Structures, 2003. **81**(17): p. 1715-1725.

39. Banks, A., J. Vincent, and C. Anyakoha, *A review of particle swarm optimization. Part I: background and development.* Natural Computing, 2007. **6**(4): p. 467-484.

40. Ladson, C.L. and C.W. Brooks, *Development of a computer program to obtain ordinates for NACA 4-Digit, 4-Digit Modified, 5-Digit and and 16-series airfoils*. 1975, National Aeronautics and Space Administration: Washington, D.C.

41. Stack, J. and A.E. Von Doenhoff, *Tests of 16 Related Airfoils at High Speeds* 1934, NACA.

42. Ross, P.J., *Taguchi techniques for quality engineering: loss function, orthogonal experiments, parameter and tolerance design.* 1988.

43. Roy, S. and U.K. Saha, *Wind tunnel experiments of a newly developed two-bladed Savonius-style wind turbine*, in *Applied Energy*. 2015. p. 117-125.

44. Almohammadi, K.M., et al., *Computational fluid dynamics (CFD) mesh independency techniques for a straight blade vertical axis wind turbine.* Energy, 2013. **58**(0): p. 483-493.

45. In-Ae, Y. and Y. Jurng-Jae, *A proposal for a site location planning model of environmentally friendly urban energy supply plants using an environment and energy geographical information system (E-GIS) database (DB) and an artificial neural network (ANN).* Applied Energy, 2014. **119**: p. 99-117.

46. Howell, R., et al., *Wind tunnel and numerical study of a small vertical axis wind turbine.* Renewable Energy, 2010. **35**(2): p. 412-422.

47. Li, C., et al., *2.5D large eddy simulation of vertical axis wind turbine in consideration of high angle of attack flow.* Renewable Energy, 2013. **51**(0): p. 317-330.

48. Afungchui, D., B. Kamoun, and A. Helali, *Vortical structures in the wake of the savonius wind turbine by the discrete vortex method*, in *Renewable Energy*. 2014. p. 174-179.

49. Ward, A. and J. Jorba, *Harmonic buffeting in a high-altitude ridge-mounted triblade Horizontal Axis Wind Turbine.* Journal of Wind Engineering and Industrial Aerodynamics, 2013. **121**: p. 106-115.

50. Borg, M. and M. Collu, *A comparison between the dynamics of horizontal and vertical axis offshore floating wind turbines.* Philosophical Transactions of the Royal Society a-Mathematical Physical and Engineering Sciences, 2015. **373**(2035).

51. Amet, E., et al., *2D Numerical Simulations of Blade-Vortex Interaction in a Darrieus Turbine.* Journal of Fluids Engineering-Transactions of the Asme, 2009. **131**(11).

52. McLaren, K.W., *A numerical and experimental study of unsteady loading of high solidty vertical axis wind turbines*, in *Mechanical Engineering*. 2011, McMaster University: Hamilton, Ontario.

53. Fiedler, A.J. and S. Tullis, *Blade offset and pitch effects on a high solidity vertical axis wind turbine.* Wind Engineering, 2009. **33**(3): p. 237-246.

Table 1 Relationship between values of d_1 and values of m

m	d_1
0.2	0.2
0.3	0.234
s0.4	0.315
0.5	0.465
0.6	0.700

Table 2 Relationship between leading-edge index number and values of a_0

Leading-edge index number	a_0
0	0
6	0.2969
9	0.514246

Table 3 Investigated factors and levels

Factors \ Levels		1	2	3	4
Thickness-chord ratio	Factor A	15	18	21	24
Leading-edge index	Factor B	0	3	6	9
Maximum thickness in tenths of chord	Factor C	2	3	4	5

Table 4 Orthogonal list $L_{16}(4^5)$

Column No. / Test No.	1	2	3	4	5
1	1(15)	1(0)	1(2)	1	1
2	1(15)	2(3)	2(3)	2	2
3	1(15)	3(6)	3(4)	3	3
4	1(15)	4(9)	4(5)	4	4
5	2(18)	1(0)	2(3)	3	4
6	2(18)	2(3)	1(2)	4	3
7	2(18)	3(6)	4(5)	1	2
8	2(18)	4(9)	3(4)	2	1
9	3(21)	1(0)	3(4)	4	2
10	3(21)	2(3)	4(5)	3	1
11	3(21)	3(6)	1(2)	2	4
12	3(21)	4(9)	2(3)	1	3
13	4(24)	1(0)	4(5)	2	3
14	4(24)	2(3)	3(4)	1	4
15	4(24)	3(6)	2(3)	4	1
16	4(24)	4(9)	1(2)	3	2

Table 5 A detailed summary of the CFD simulation on VAWTs (1)

Author	Hamada,K 2008. [42]	Amet,E. 2009, [43]	Howell,R., 2010 [44]	RaciticastIli,M 2011[45]	Castelli,M.R 2012[31]
Dimension	**2D,3D**	**2D**	**2D,3D**	**2D,3D**	**2D**
Blade profile	**NACA0022**	**NACA0018**	**NACA 0022**	**NACA0021**	**NACA0021**
Diameter	**2.5m**	**0.12m**	**0.3m**	**0.4m**	**0.4m**
Chord length	**200mm**	**20mm**	**100mm**	**85.8mm**	**85.8mm**
Mesh number	**3D 2million**	**2D 160,000**	**2D&3D 1.3 million**	**2D&3D 600000~1000000**	**2D 13106~91105**
Nodes on blades	*	**188**	*	**3600**	*
Height of the first layer	*	**25um**	*	*	*
Mesh type	**Tetrahedron**	**Structured**	**Tetrahedron**	**unstructured**	**unstructured**
Re or velocity	**1150000**	**10000**	**39000**	**9 m/s**	**Low 9m/s**
Domain size	**50c*30c**	**30C**	**16D**	**80D**	**80D**
Degree at each step	*	**0.25°**	*	**4°**	**1°**
Turbulence model	**RNG** $K-\varepsilon$	$K-\omega$	**RNG** $K-\varepsilon$	$K-\varepsilon$	**SST** $K-\omega$, **Realizable** $K-\varepsilon$,
Y+ and Wall treatment	**Standard**	**Y+ close to 1**	**Y+<10, Standard**	**enhanced**	**enhanced**
Algorithm	*	*	*	*	*
Interpolating scheme	**Second-order upwind**	**Third-order upwind**	**Second-order upwind**	**Second-order upwind**	**Upwind Downwind**
Inlet	**Velocity inlet**	**Velocity inlet**	**Velocity inlet**	**Velocity inlet**	**Velocity inlet**
Outlet	**Outflow**	**Pressure outlet**	**Outflow**	**Pressure outlet**	**Pressure outlet**

Table 6 A detailed summary of the CFD simulation on VAWTs (2)

Author	Li, Chao 2013[46]	Biadgo 2013[47]	Rosario,L,etal 2014[48]	Wekesa,D.W. et al 2015[49]	Edwards, Jonathan M 2015[50]
Dimension	**2D,2.5D**	**2D**	**2D**	**2D**	**2D**
Blade profile	**NACA0018**	**NACA0012**	**NACA0015 NACA4518**	**NACA0022**	**NACA0022**
Diameter	*	**4m**	**2.5m&0.6m**	**0.35m**	**0.35m**
Chord length	**200mm**	**200mm**	**0.4m&0.1m**	**0.04m**	**0.04m**
Mesh number	**2D, 2.5D 131690, 5267600**	**2D 83641**	**2D 700000**	**2D ***	**2D ***
Nodes on blades	*	*	*	*	**400**
Height of the first layer	**2.05mm**	*	*	*	*
Mesh type	**hexahedron**	**Structured**	**Unstructured**	**Structured**	**Structured O-type**
Re or velocity	**10m/s**	**5 m/s**	**10m/s**	**10m/s**	**7m/s**
Domain size	**30C**	*	**2.5D*9D**	**60C*120C**	*
Degree at each step	**0.5°**	*	**$5*10^{-4}$s**	**$1*10^{-5}$s**	**0.5°,1°**
Turbulence model	**SST LES**	**RNG $K-\varepsilon$**	**Transition SST, SST**	**Transition SST SST $K-\omega$**	**SST $K-\omega$**
Y+ and Wall treatment	**Y+≥1**	**Standard**	**Y+<1**	**Y+<1**	**Y+<2.2**
Algorithm	*	**Simple**	**PISO**	**Simple**	*
Interpolating scheme	**Second-order upwind third-order MUSCL**	*	**Second-order Upwind**	**Second-order Upwind**	**Second-order Upwind**
Inlet	**Velocity inlet**	**Velocity inlet**	**Velocity inlet**	**Velocity inlet**	**Velocity inlet**
Outlet	**Outflow**	**Pressure outlet**	**Pressure outlet**	**Pressure outlet**	**Pressure outlet**

Table 7 Maximum CP results of the orthogonal method for 16 NACA 4-digital-modified airfoils

Column No. / *Test No.*	*1* *A*	*2* *B*	*3* *C*	*Maximum power*
1	1(15)	1(0)	1(2)	0.362775
2	1(15)	2(3)	2(3)	0.38175
3	1(15)	3(6)	3(4)	0.413975
4	1(15)	4(9)	4(5)	0.4033
5	2(18)	1(0)	2(3)	0.327225
6	2(18)	2(3)	1(2)	0.400825
7	2(18)	3(6)	4(5)	0.38725
8	2(18)	4(9)	3(4)	0.39585
9	3(21)	1(0)	3(4)	0.31264
10	3(21)	2(3)	4(5)	0.35136
11	3(21)	3(6)	1(2)	0.37565
12	3(21)	4(9)	2(3)	0.374
13	4(24)	1(0)	4(5)	0.31856
14	4(24)	2(3)	3(4)	0.338725
15	4(24)	3(6)	2(3)	0.34975
16	4(24)	4(9)	1(2)	0.308675
K_1	1.5618	1.3212	1.447925	
K_2	1.51115	1.47266	1.432725	

Table 7 Maximum CP results of the orthogonal method for 16 NACA 4-digital-modified airfoils (continued)

Column No. / ***Test No.***	***1*** ***A***	***2*** ***B***	***3*** ***C***	***Maximum power***
K_3	1.41365	1.526625	1.46119	
K_4	1.31571	1.481825	1.46047	
κ_1	0.39045	0.3303	0.361981	
κ_2	0.377788	0.368165	0.358181	
κ_3	0.353413	0.381656	0.365298	
κ_4	0.328928	0.370456	0.365118	
Max(κ_i)-Min(κ_i)	0.061522	0.051356	0.007117	
Optimal level	A1	B3	C3	

Table 8 Maximum and average C_P for maximum thickness in tenths of chord (NACA 4-digital-modifed airfoil)

	Maximum C_P	Average C_P
NACA 0015-62	0.41655	0.257
NACA 0015-63	0.4045	0.232
NACA 0015-64	0.41075	0.252
NACA 0015-65	0.39875	0.234

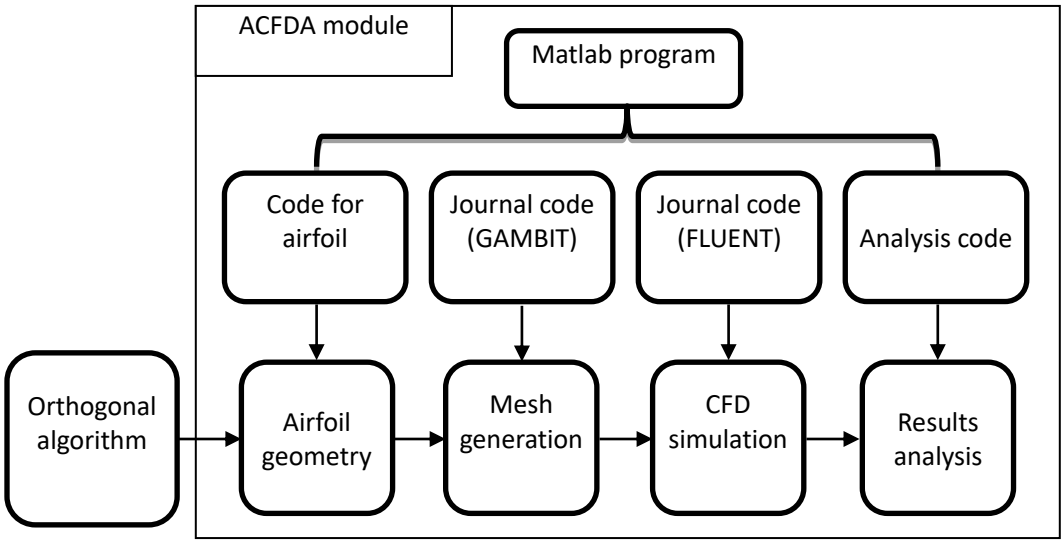

Figure 1 Orthogonal algorithm and ACFDA module

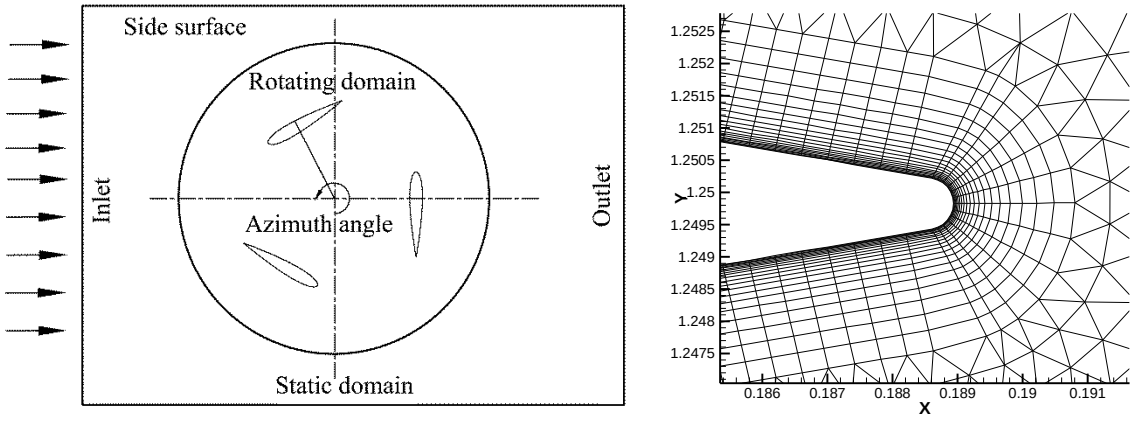

Figure 2 Schematic of computational domain

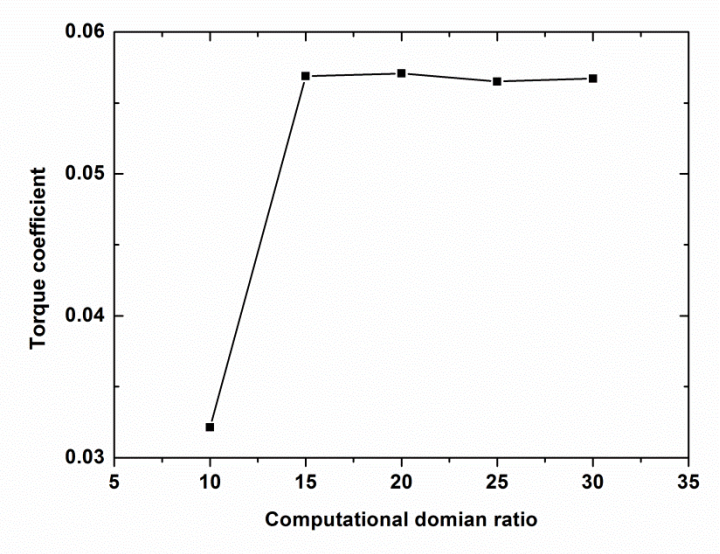

Figure 3 Computational domain ratio

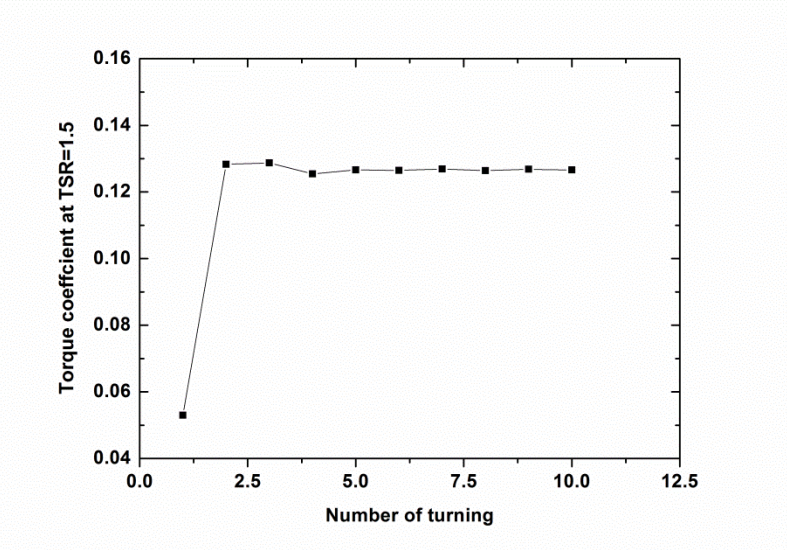

Figure 4 Number of turns

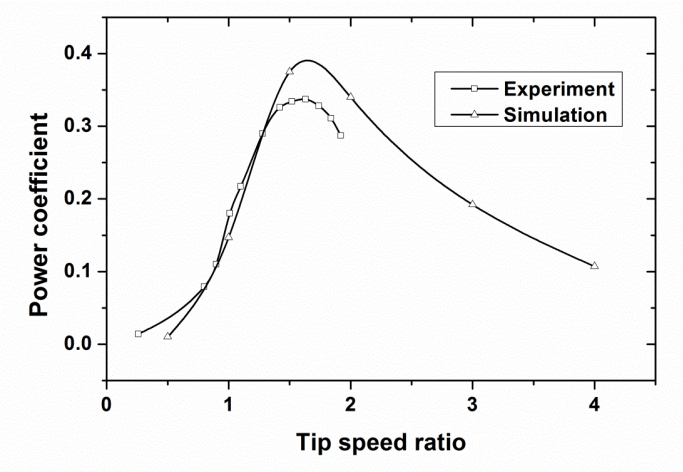

Figure 5 Validation of the simulated results

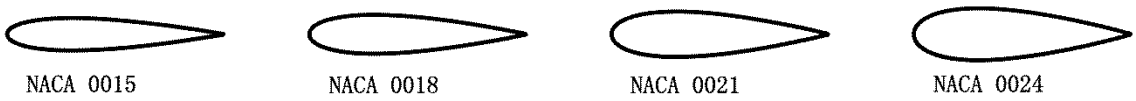

Figure 6 Four NACA 4-digital airfoils with different thickness-chord ratios

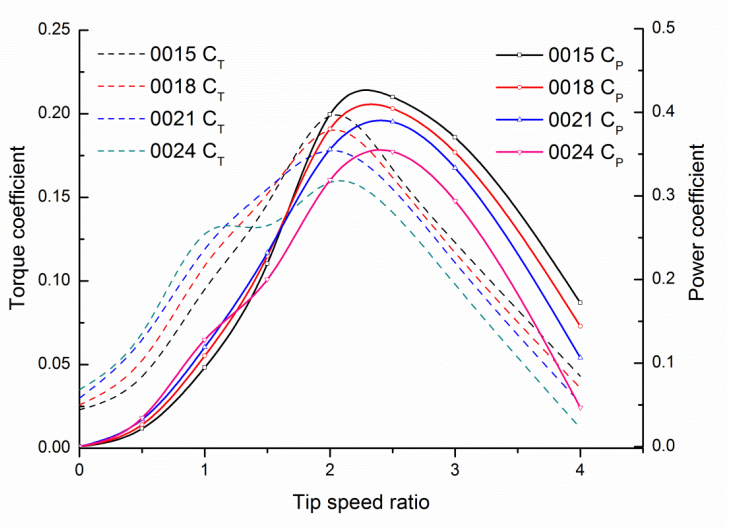

Figure 7 Effect of the thickness-chord ratio on the performance of the rotor (NACA 4-digital airfoil family)

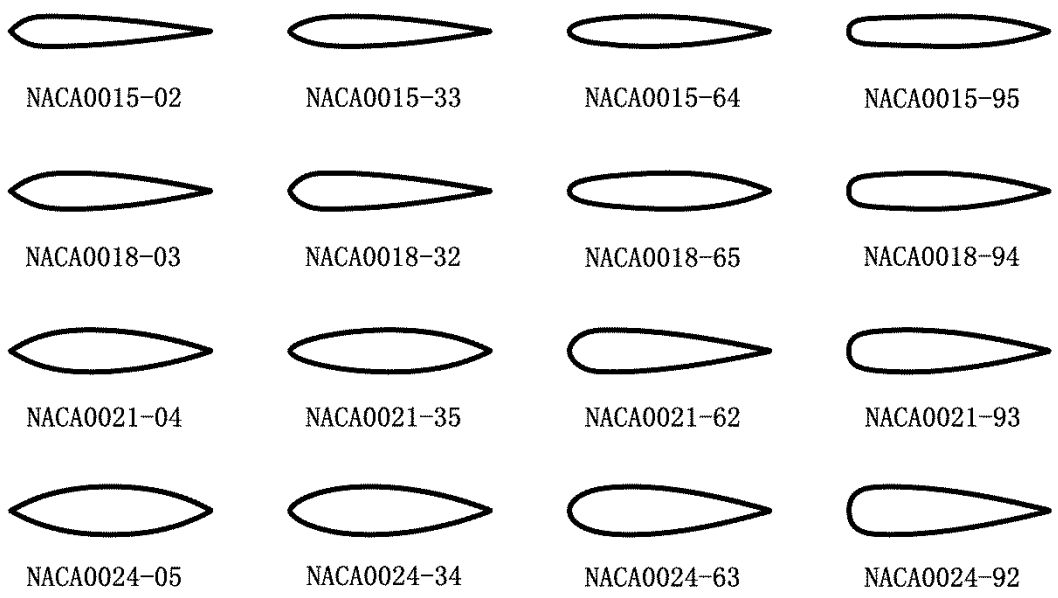

Figure 8 Sixteen NACA 4-digital-modified airfoils for the orthogonal algorithm

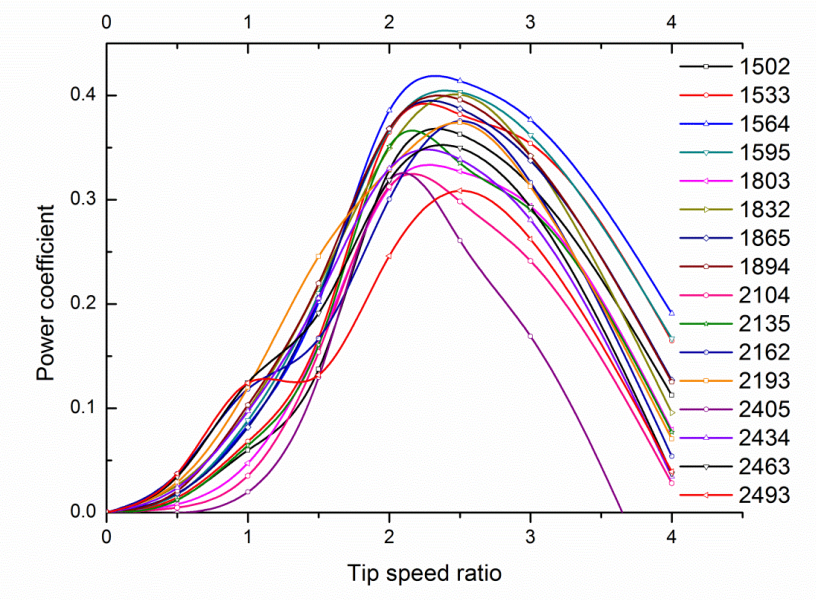

Figure 9 Power curves of Sixteen NACA 4-digital-modified airfoils

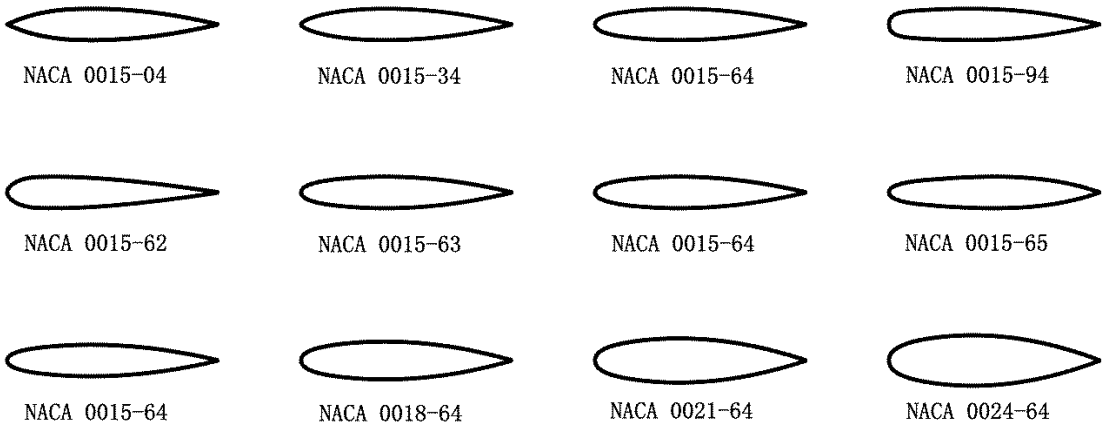

Figure 10 Twelve NACA 4-digital-modified airfoils studied by OFAAT algorithm

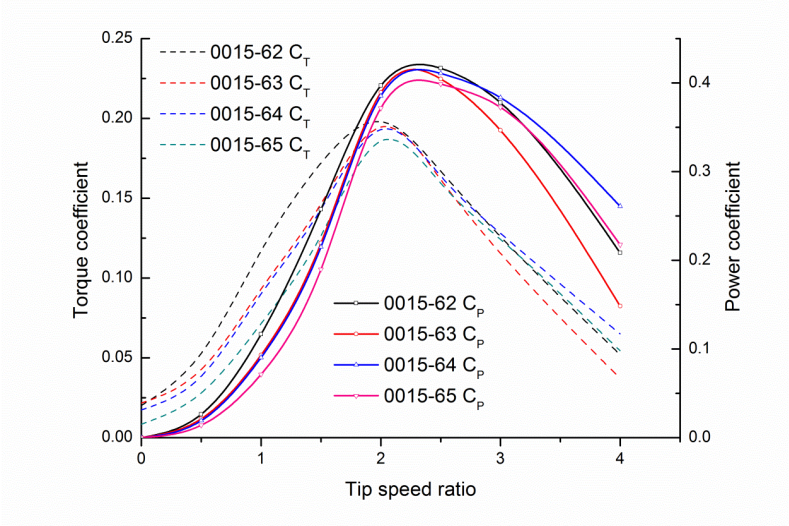

Figure 11 The effect of the MTITOC (NACA 4-digital-modified airfoil)

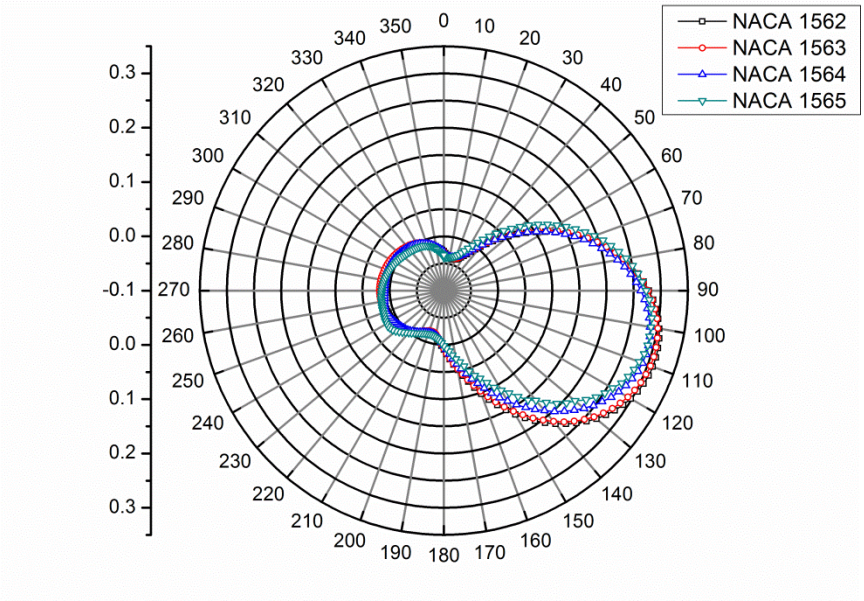

Figure 12 Instantaneous CT as a function of azimuth angle (MTITOC)

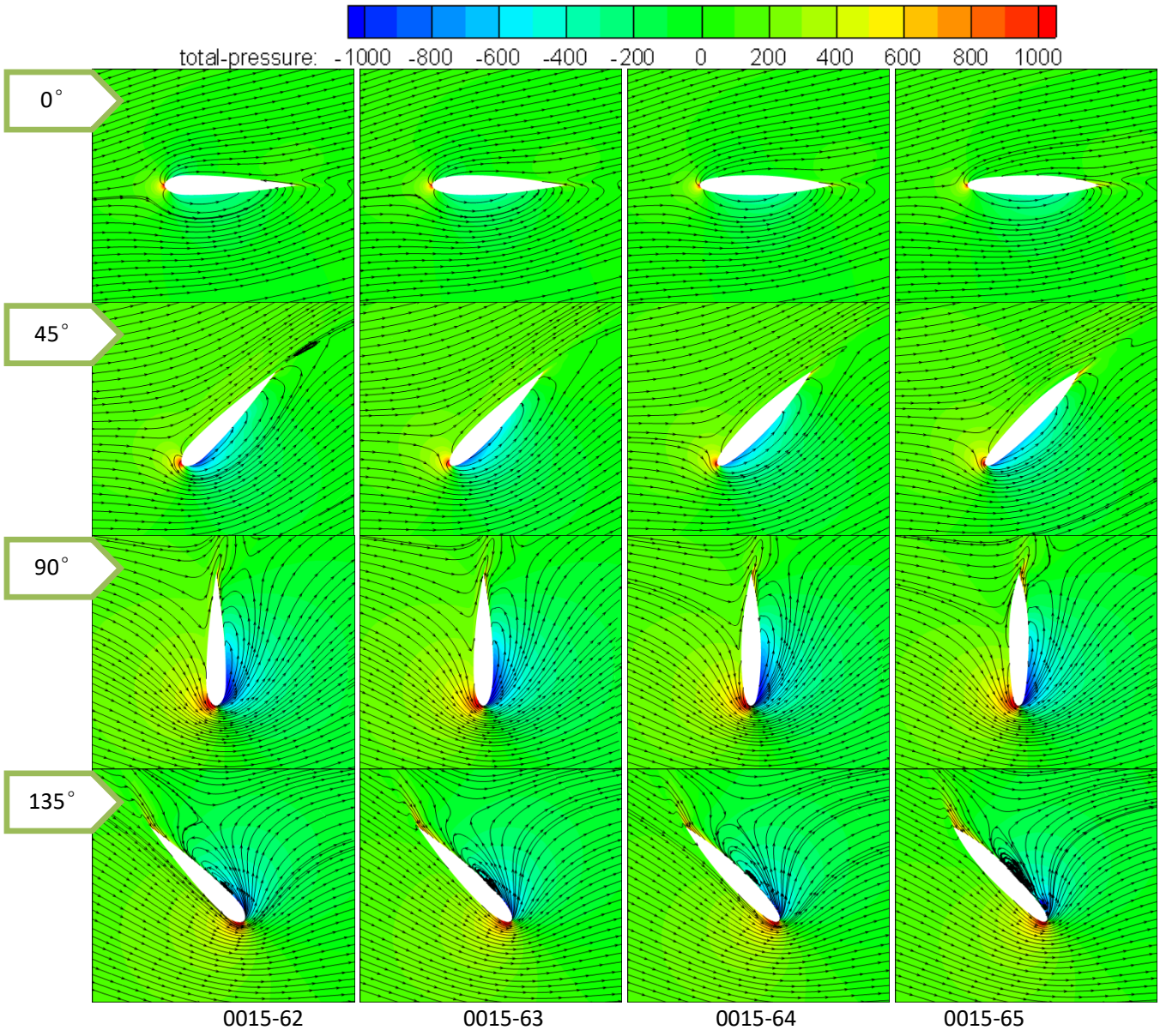

Figure 13 Instantaneous contour of pressure coefficient and streamline for blade No.1 at TSR=2.5 in upwind zone (MTITOC)

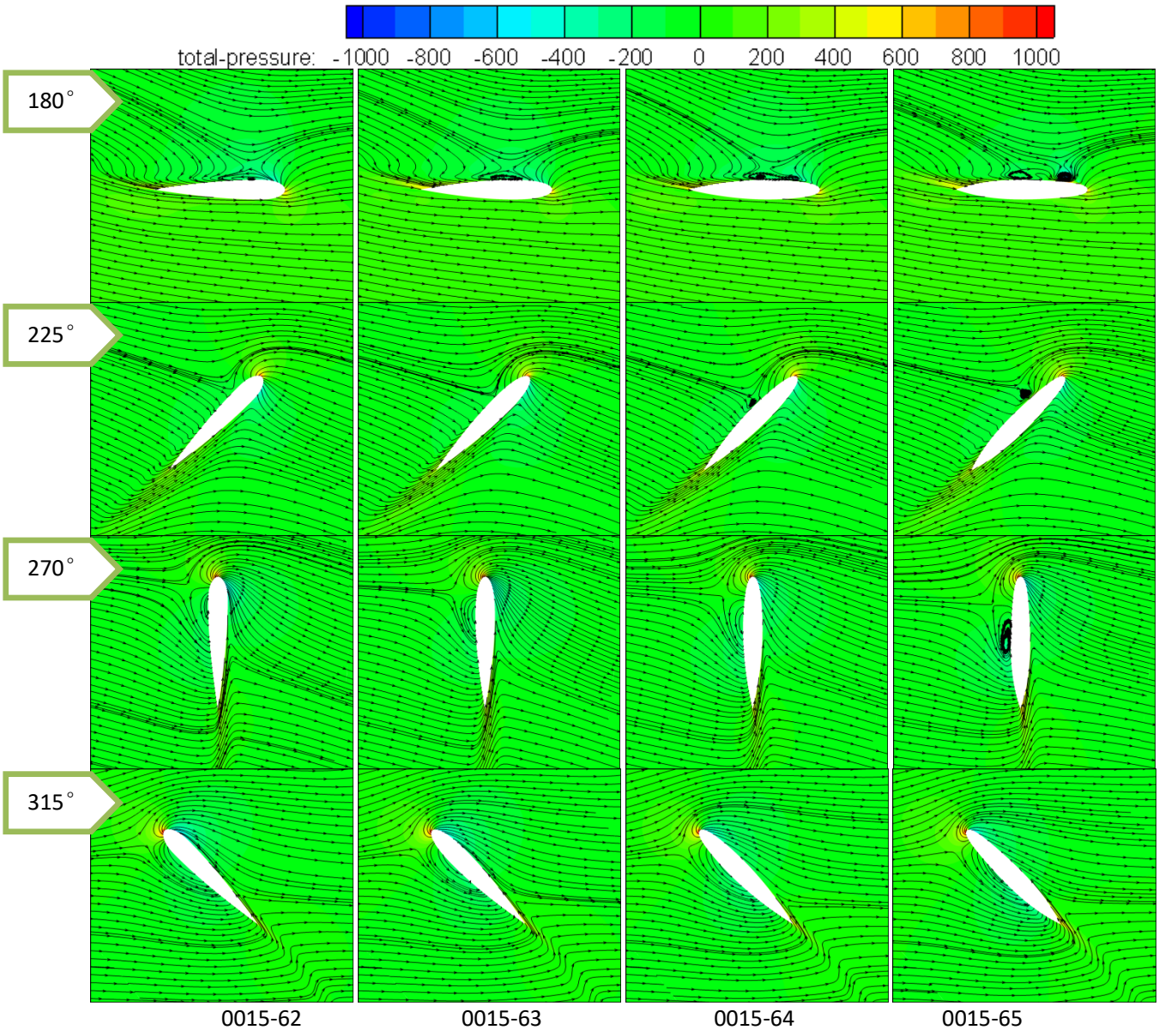

Figure 14 Instantaneous contour of pressure coefficient and streamline for blade No.1 at TSR=2.5 in downwind zone (MTITOC)

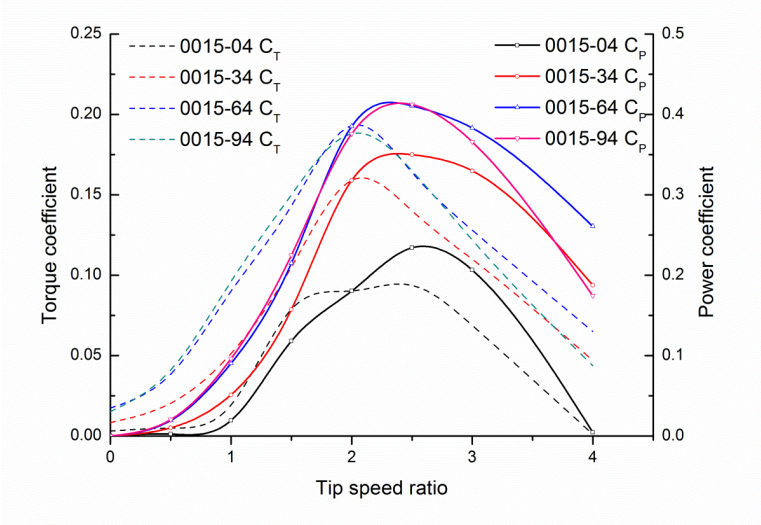

Figure 15 The effect of the leading-edge number (NACA 4-digital-modified airfoil)

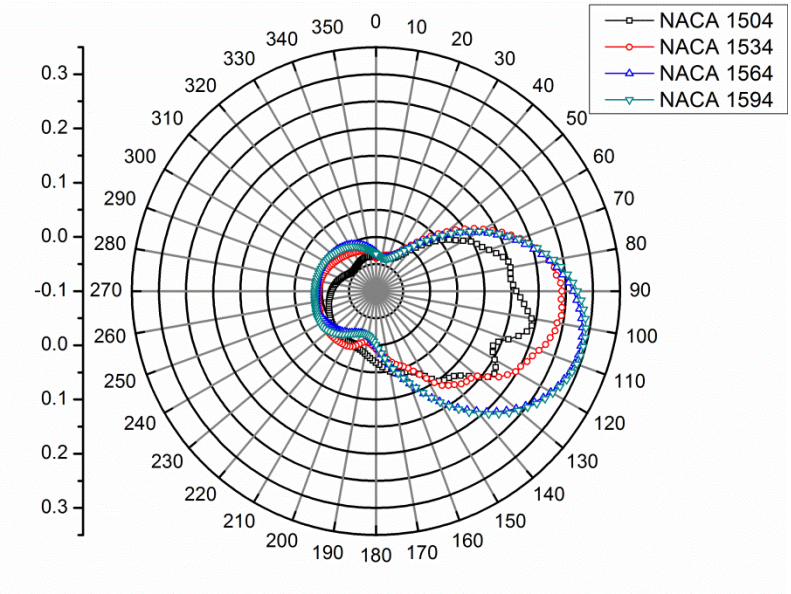

Figure 16 Instantaneous CT as a function of azimuth angle (LEN)

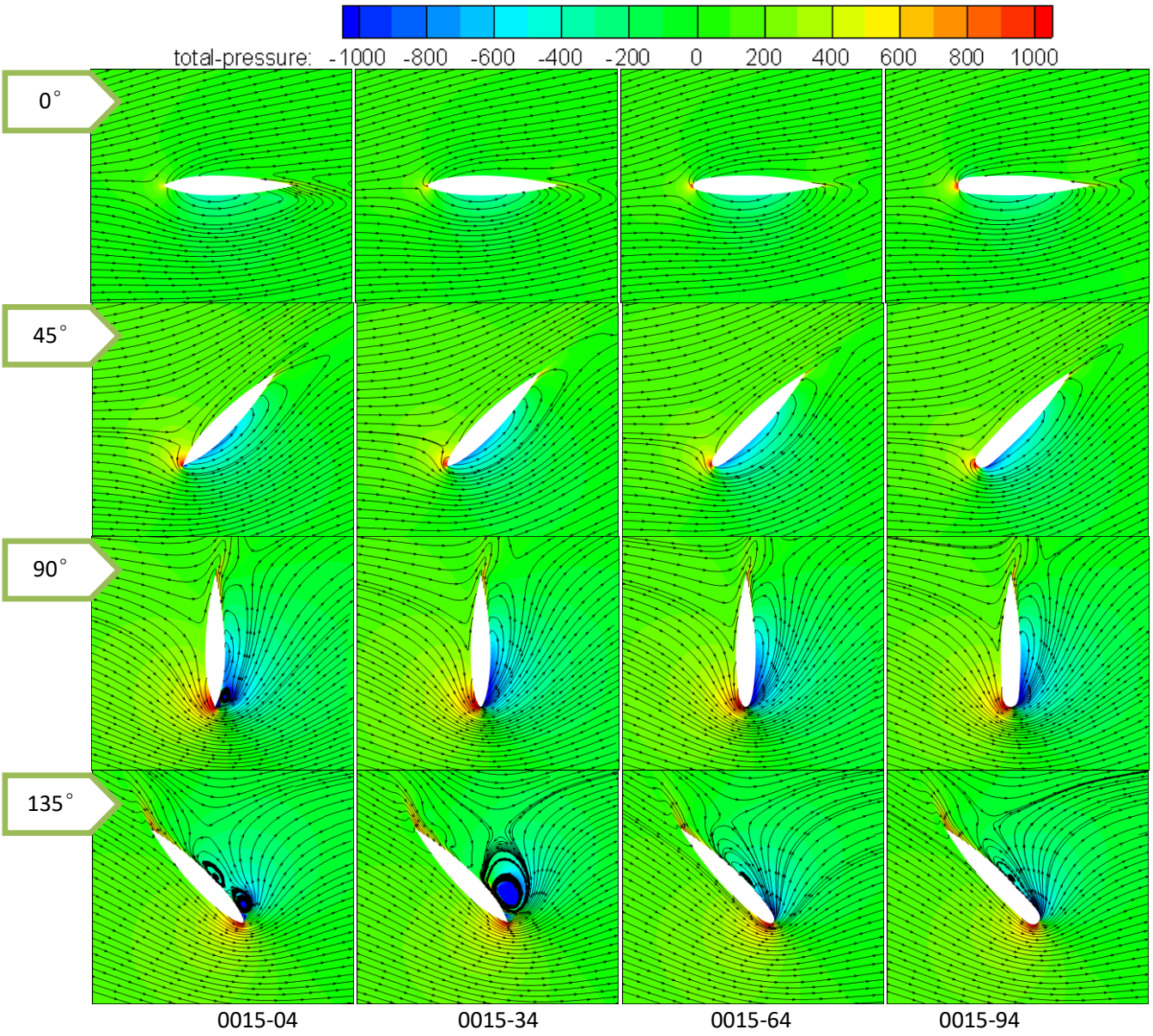

Figure 17 Instantaneous contour of pressure coefficient and streamline for blade No.1 at TSR=2.5 in upwind zone (LEN)

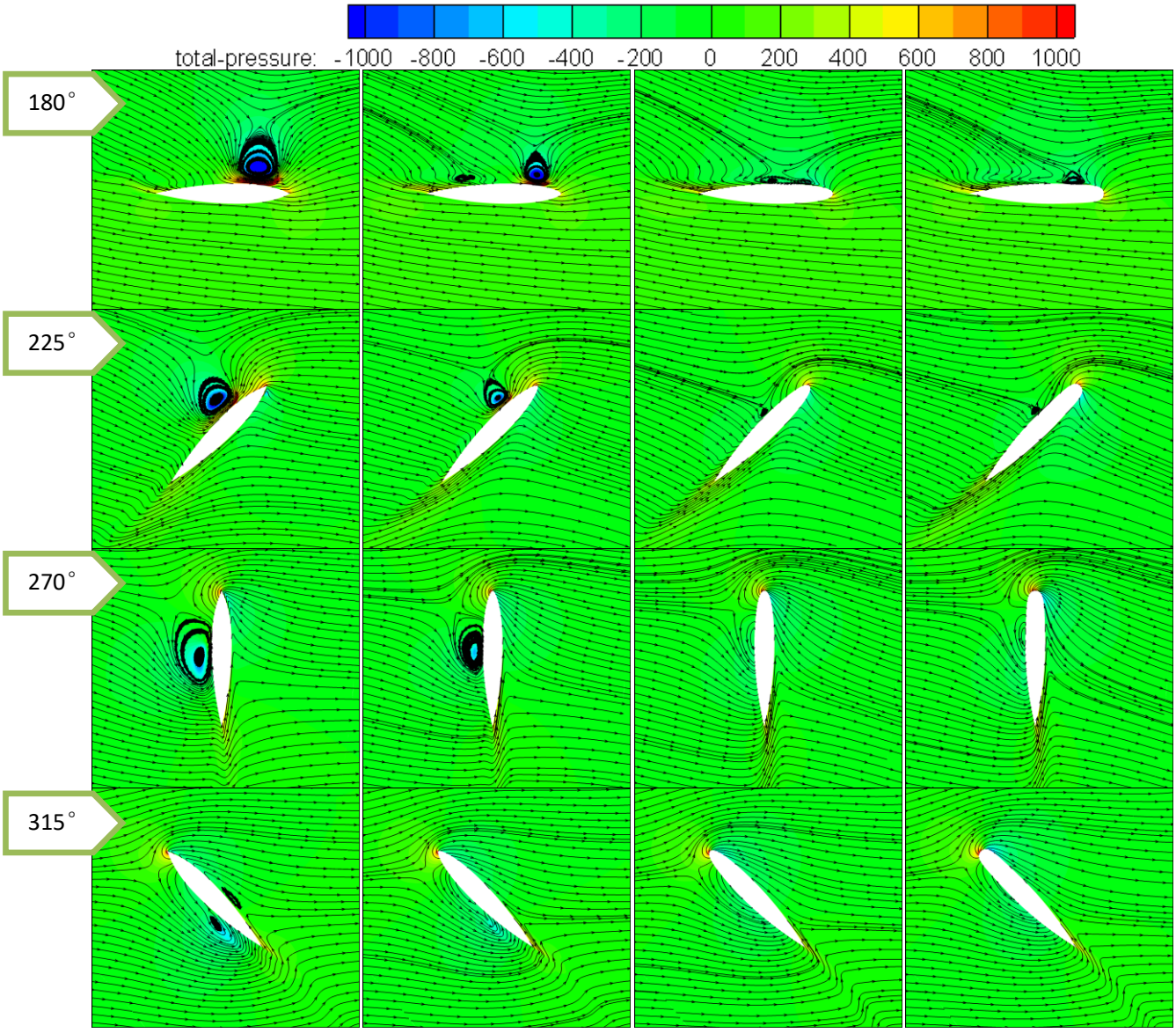

Figure 18 Instantaneous contour of pressure coefficient and streamline for blade No.1 at TSR=2.5 in downwind zone (LEN)

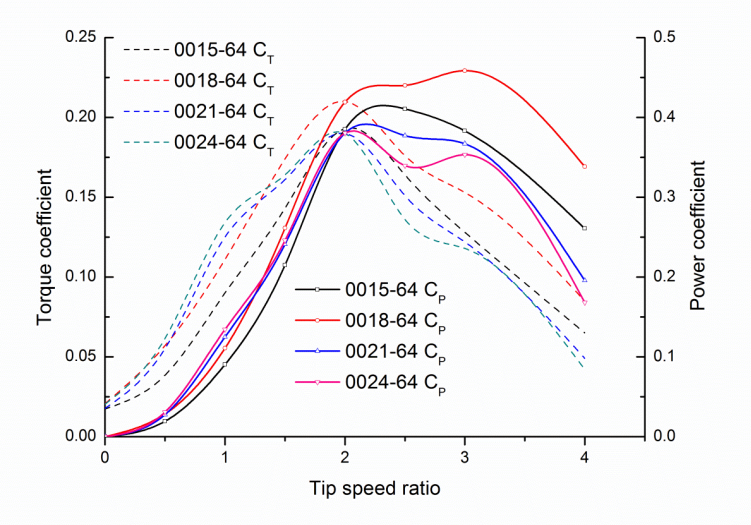

Figure 19 The effect of thickness-chord ratio (NACA 4-digital-modified airfoil)

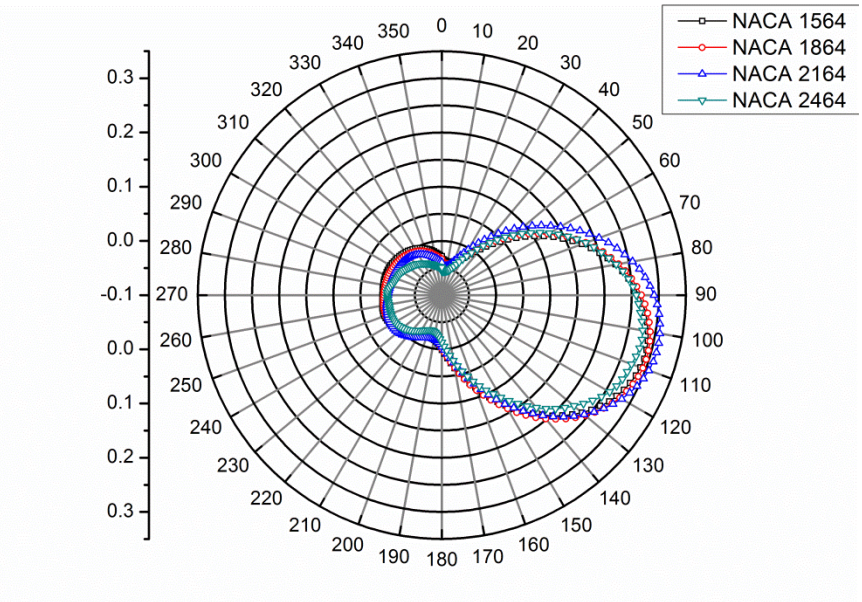

Figure 20 Instantaneous C_T as a function of azimuth angle (TCR)

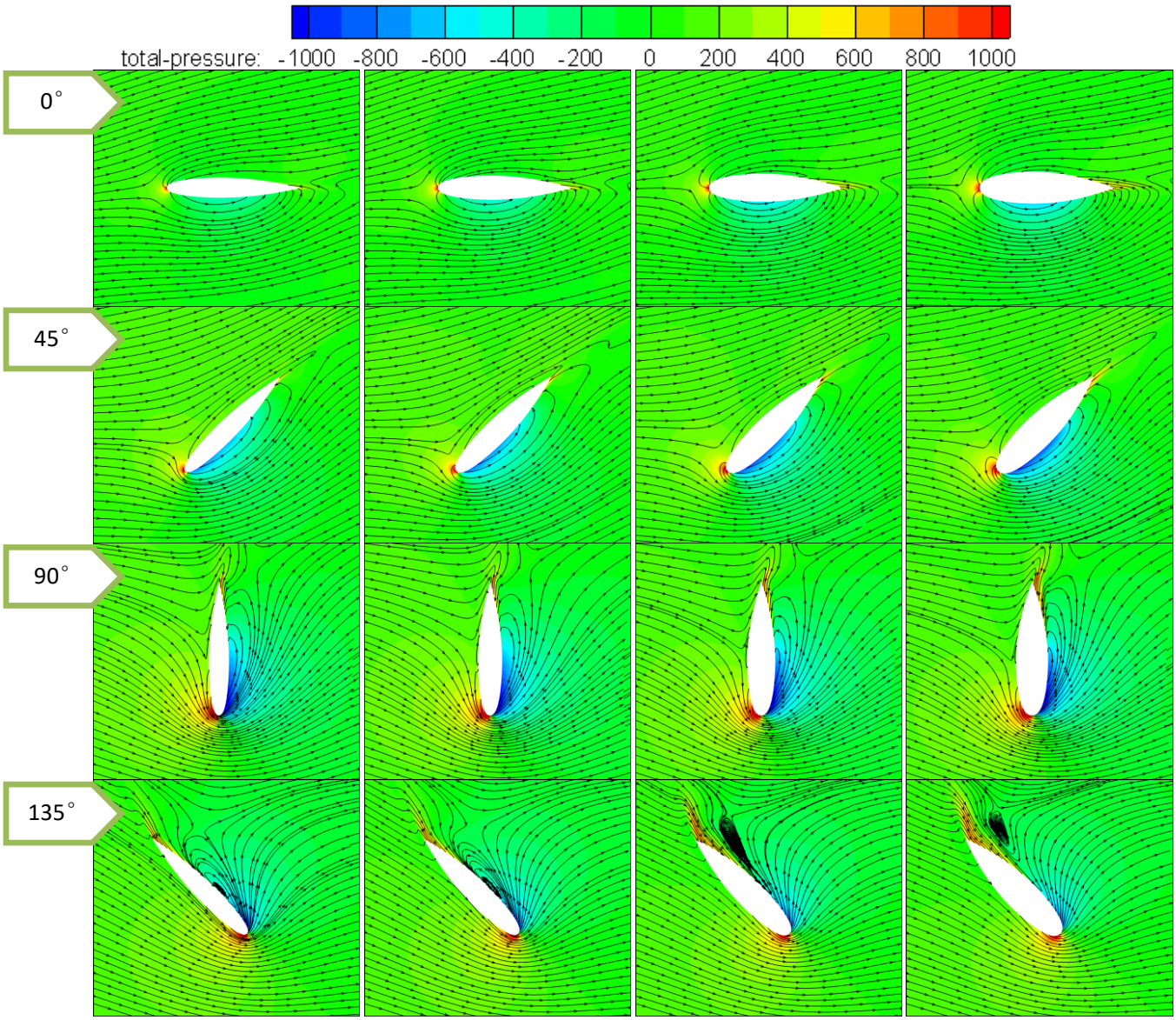

Figure 21 Instantaneous contour of pressure coefficient and streamline for blade No.1 at TSR=2.5 in upwind zone (TCR)

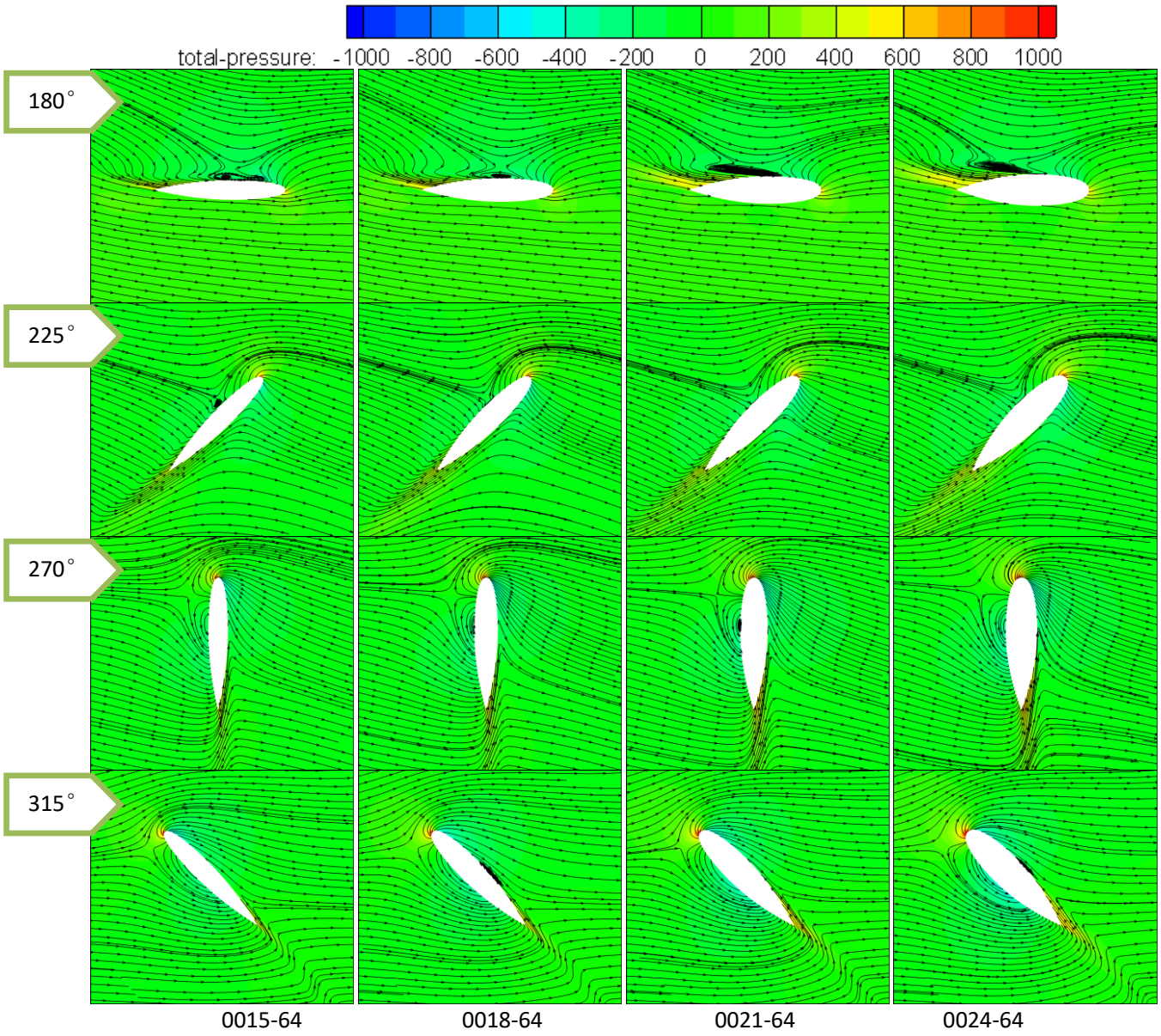

Figure 22 Instantaneous contour of pressure coefficient and streamline for blade No.1 at TSR=2.5 in downwind zone (TCR)